Eidgenössische Technische Hochschule Zürich

Ecole polytechnique fédérale de Zurich
Politecnico federale di Zurigo
Swiss Federal Institute of Technology Zurich

Constraint preserving schemes using potential-based fluxes
III. Genuinely multi-dimensional central schemes for MHD equations

S. Mishra and E. Tadmor*

Research Report No. 2009-33
November 2009

Seminar für Angewandte Mathematik
Eidgenössische Technische Hochschule
CH-8092 Zürich
Switzerland

*Department of Mathematics, Institute for Physical Sciences and Technology (IPST), University of Maryland, College Park, MD 20742-4015, USA

CONSTRAINT PRESERVING SCHEMES USING POTENTIAL-BASED FLUXES. III. GENUINELY MULTI-DIMENSIONAL CENTRAL SCHEMES FOR MHD EQUATIONS.

SIDDHARTHA MISHRA AND EITAN TADMOR

Abstract. We design efficient numerical schemes for approximating the MHD equations in multi-dimensions. Numerical approximations must be able to deal with the complex wave structure of the MHD equations and the divergence constraint. We propose schemes based on the genuinely multi-dimensional (GMD) framework of [31, 32]. The schemes are formulated in terms of *vertex-centered potentials*. A suitable choice of the potential results in GMD schemes that preserve a discrete version of divergence. First- and second-order divergence preserving GMD schemes are tested on a series of benchmark numerical experiments. They demonstrate the computational efficiency and robustness of the GMD schemes.

1. Introduction

Modeling of plasmas lies at the core of many interesting problems in astrophysics, solar physics, electrical and aerospace engineering. Macroscopic plasma dynamics is characterized by the interaction of the moving plasma with the magnetic field. This model is often by the equations of ideal MagnetoHydrodynamics (MHD). In two space dimensions, the MHD equations are

$$\mathbf{U}_t + \mathbf{f}(\mathbf{U})_x + \mathbf{g}(\mathbf{U})_y = 0, \quad (x,y,t) \in \mathbb{R}\times\mathbb{R}\times\mathbb{R}_+ \tag{1.1}$$

for

$$\mathbf{U} = \begin{pmatrix} \rho \\ \rho u_1 \\ \rho u_2 \\ \rho u_3 \\ B_1 \\ B_2 \\ B_3 \\ E \end{pmatrix}, \mathbf{f} = \begin{pmatrix} \rho u_1 \\ \rho(u_1)^2 + \widetilde{p} - \frac{1}{2}(B_1)^2 \\ \rho u_1 u_2 - B_1 B_2 \\ \rho u_1 u_3 - B_1 B_3 \\ 0 \\ -(u_2 B_1 - u_1 B_2) \\ u_1 B_3 - u_3 B_1 \\ (E+\widetilde{p})u_1 - (\mathbf{u}\cdot\mathbf{B})B_1 \end{pmatrix}, \mathbf{g} = \begin{pmatrix} \rho u_2 \\ \rho u_1 u_2 - B_1 B_2 \\ \rho(u_2)^2 + \widetilde{p} - \frac{1}{2}(B_2)^2 \\ \rho u_1 u_3 - B_1 B_3 \\ u_2 B_1 - u_1 B_2 \\ 0 \\ u_2 B_3 - u_3 B_2 \\ (E+\widetilde{p})u_2 - (\mathbf{u}\cdot\mathbf{B})B_2 \end{pmatrix}. \tag{1.2}$$

Density of the plasma is denoted as ρ and $\mathbf{u} = \{u_1, u_2, u_3\}$, $\mathbf{B} = \{B_1, B_2, B_3\}$ are the velocity and magnetic fields, respectively. E is the total energy and $\widetilde{p}$ is the total pressure:

$$\widetilde{p} = p + \frac{1}{2}|\mathbf{B}|^2,$$

with p being the thermal pressure. The unknowns are related by an ideal gas equation of state:

$$E = \frac{p}{\gamma - 1} + \frac{1}{2}(\rho|\mathbf{u}|^2 + |\mathbf{B}|^2) \tag{1.3}$$

for gas constant γ.

Date: November 10, 2009.

1991 *Mathematics Subject Classification.* 65M06,35L65.

Key words and phrases. multidimensional evolution equations, magentohydrodynamics, constraint transport, central difference schemes, potential-based fluxes.

Acknowledgment. The work on this paper was started when S.M. visited the Center of Scientific Computation and Mathematical Modeling (CSCAMM) and he thanks CSCAMM and all its members for the excellent hospitality and facilities. E. T. Research was supported in part by NSF grant 07-07949 and ONR grant N00014-91-J-1076.

The ideal MHD equations (1.1) combine conservation laws for mass, momentum and energy with the Magnetic induction equations (a special form of the Maxwell's equations),

$$\mathbf{B}_t + \mathrm{curl}(\mathbf{B}\times\mathbf{u}) = 0, \quad (x,y,t)\in\mathbb{R}\times\mathbb{R}\times\mathbb{R}_+. \tag{1.4}$$

A detailed derivation of (1.1) is described in [39]. Applying the divergence operator to both sides of (1.4), we obtain the divergence constraint:

$$(\mathrm{div}\mathbf{B})_t \equiv 0. \tag{1.5}$$

Since magnetic monopoles have not been observed in nature, the initial magnetic field is assumed to be divergence free. The divergence constraint (1.5) implies that the divergence of the magnetic field remains zero.

The ideal MHD equations are an example for multi-dimensional systems of conservation laws with an intrinsic constraint. The eigenvalues of the flux Jacobians of (1.1) are real [40] and the system is hyperbolic. However, the system is *non-strictly* hyperbolic as the eigenvalues fail to be distinct.

Even for smooth initial data, the solutions of a non-linear system like (1.1) develop discontinuities in the form of shock waves and contact discontinuities. Hence, solutions of (1.1) are sought in the weak sense. The non-strict hyperbolicity and non-convexity of the MHD equations leads to a complex shock structure, consisting of intermediate and compound shocks [41]. Very few theoretical results for the MHD equations (even in one space dimension) are currently available.

1.1. **Finite-volume schemes.** Finite-volume methods are among the most widely used numerical methods for the approximate solution of systems of conservation laws such as the mhd equations (1.1), see [26, 44] and the references therein. In a finite volume approximation, the computational domain is discretized into cells and an integral form of the conservation law (1.1) is discretized on each cell. This method relies on constructing suitable numerical fluxes in the normal direction, across each cell interface. For simplicity, we consider a uniform Cartesian mesh with mesh sizes $\Delta x, \Delta y$ in the x- and y- directions respectively. It consists of the discrete cells, $\mathcal{C}_{i,j} := [x_{i-\frac{1}{2}}, x_{i+\frac{1}{2}}) \times [y_{j-\frac{1}{2}}, y_{j+\frac{1}{2}})$, centered at the mesh points $(x_i, y_j) = (i\Delta x, j\Delta y)$, $(i,j)\in\mathbb{Z}^2$. The cell average of $\mathbf{U}$ over $\mathcal{C}_{i,j}$ (at time t), denoted as $\mathbf{U}_{i,j}(t)$, is updated with the semi-discrete scheme [26, 44]:w

$$\frac{d}{dt}\mathbf{U_{i,j}} = -\frac{1}{\Delta x}\big(\mathbf{F}_{i+\frac{1}{2},j} - \mathbf{F}_{i-\frac{1}{2},j}\big) - \frac{1}{\Delta y}\big(\mathbf{G}_{i,j+\frac{1}{2}} - \mathbf{G}_{i,j-\frac{1}{2}}\big). \tag{1.6}$$

The time dependence of all the quantities in the above expression is suppressed for notational convenience. Classical first-order schemes employ two-point numerical fluxes of the form

$$\mathbf{F}_{i+\frac{1}{2},j} = \mathbf{F}(\mathbf{U}_{i,j}, \mathbf{U}_{i+1,j}), \quad \mathbf{G}_{i,j+\frac{1}{2}} = \mathbf{G}(\mathbf{U}_{i,j}, \mathbf{U}_{i,j+1}). \tag{1.7}$$

A canonical example is provided by the first-order Rusanov numerical flux:

$$\begin{aligned}
\mathbf{F}_{i+\frac{1}{2},j} &= \frac{1}{2}\big(\mathbf{f}(\mathbf{U}_{i,j}) + \mathbf{f}(\mathbf{U}_{i+1,j})\big) - \max\{|\alpha_{i,j}|, |\alpha_{i+1,j}|\}\mathbf{L}\big(\mathbf{U}_{i+1,j} - \mathbf{U}_{i,j}\big),\\
\mathbf{G}_{i,j+\frac{1}{2}} &= \frac{1}{2}\big(\mathbf{g}(\mathbf{U}_{i,j}) + \mathbf{g}(\mathbf{U}_{i,j+1})\big) - \max\{|\beta_{i,j}|, |\beta_{i,j+1}|\}\mathbf{Id}\big(\mathbf{U}_{i,j+1} - \mathbf{U}_{i,j}\big).
\end{aligned} \tag{1.8}$$

for the 8×8 identity matrix $\mathbf{Id}$ and the scaling matrix $\mathbf{L}$:

$$L = \mathrm{diag}\{1,1,1,1,1,-1,1,1\}.$$

The sixth component $\mathbf{f}_6$ of $\mathbf{f}$ has a negative sign, leading to the special form of the scaling matrix $\mathbf{L}$. The $\alpha_{i,j}$ and $\beta_{i,j}$ in (1.8) are the maximal eigenvalues of the Jacobians $\mathbf{A} = \partial_{\mathbf{U}}\mathbf{f}$ and $\mathbf{B} = \partial_{\mathbf{U}}\mathbf{g}$ respectively, for any given state $\mathbf{U}_{i,j}$, i.e,

$$\alpha = |u_1| + |c_f^x|, \quad \beta \quad = |u_2| + |c_f^y|, \tag{1.9}$$

for

$$a^2 = \frac{\gamma p}{\rho} \quad \text{and} \quad b_{1,2,3} = \frac{B_{1,2,3}}{\sqrt{\rho}}, \quad b^2 = b_1^2 + b_2^2 + b_3^2,$$

and

$$(c_f^{x,y})^2 = \frac{1}{2}\left(a^2 + b^2 + \sqrt{\left(a^2+b^2\right)^2 - 4a^2b_{1,2}^2}\right). \tag{1.10}$$

The explicit dependence on i, j in the above quantities is supressed for notational convenience. Note that the only characteristic information in the Rusanov flux is a local estimate on the wave speeds. This flux is almost Jacobian free, very simple to implement and has a very low computational cost. But its resolution is limited by the first-order accuracy. The Rusanov flux (1.8) has been used to define simple but highly effective high resolution central schemes [2, 3] for the ideal MHD equations. Other popular numerical fluxes for the MHD equations include the Roe type linearized solvers [40, 9, 39]) and HLL type solvers [30, 21, 34, 7, 17]. Detailed comparisons of different solvers are performed in [33, 18].

The first-order schemes (1.6),(1.7) can be extended to higher order accuracy by employing numerical fluxes based on wider, $2p$-point stencils, $I_{i+\frac{1}{2}} := \{i' \,|\, |i'-i-1/2| < p\}$ along the x-axis and $J_{j+\frac{1}{2}} := \{j' \,|\, |j'-j-1/2| < p\}$ along the y-axis,

$$\mathbf{F}_{i+\frac{1}{2},j} = \mathbf{F}\Big(\{\mathbf{U}_{i',j}\}_{i'\in I_{i+\frac{1}{2}}}\Big), \quad \mathbf{G}_{i,j+\frac{1}{2}} = \mathbf{G}\Big(\{\mathbf{U}_{i,j'}\}_{j'\in J_{j+\frac{1}{2}}}\Big). \tag{1.11}$$

The building blocks for such extensions are still the 2-point numerical fluxes, $\mathbf{F}(\cdot,\cdot)$ and $\mathbf{G}(\cdot,\cdot)$. As a prototype example, we recall the class of second-order schemes based on piecewise bilinear MUSCL reconstruction [25],

$$\mathbf{p}_{i,j}(x,y) := \mathbf{U}_{i,j} + \frac{\mathbf{U}'_{i,j}}{\Delta x}(x-x_i) + \frac{\mathbf{U}\backprime_{i,j}}{\Delta y}(y-y_j); \tag{1.12a}$$

Here, $\mathbf{U}'$ and $\mathbf{U}\backprime$ denote the *numerical derivatives*

$$\begin{aligned} \mathbf{U}'_{i,j} &= \text{minmod}(\mathbf{U}_{i+1,j}-\mathbf{U}_{i,j}, \frac{1}{2}(\mathbf{U}_{i+1,j}-\mathbf{U}_{i-1,j}), \mathbf{U}_{i,j}-\mathbf{U}_{i-1,j}),\\ \mathbf{U}\backprime_{i,j} &= \text{minmod}(\mathbf{U}_{i,j+1}-\mathbf{U}_{i,j}, \frac{1}{2}(\mathbf{U}_{i,j+1}-\mathbf{U}_{i,j-1}), \mathbf{U}_{i,j}-\mathbf{U}_{i,j-1}), \end{aligned} \tag{1.12b}$$

which utilize the minmod limiter

$$\text{minmod}(a,b,c) = \begin{cases} sgn(a)\min\{|a|,|b|,|c|\}, & \text{if} \quad sgn(a)=sgn(b)=sgn(c),\\ 0, \qquad \text{otherwise.} \end{cases} \tag{1.12c}$$

In this manner, one can reconstruct in each cell $\mathcal{C}_{i,j}$, the point values

$$\mathbf{U}^E_{i,j} := \mathbf{p}_{i,j}(x_{i+\frac{1}{2}}, y_j), \quad \mathbf{U}^W_{i,j} := \mathbf{p}_{i,j}(x_{i-\frac{1}{2}}, y_j), \quad \mathbf{U}^N_{i,j} := \mathbf{p}_{i,j}(x_i, y_{j+\frac{1}{2}}), \quad \mathbf{U}^S_{i,j} := \mathbf{p}_{i,j}(x_i, y_{j-\frac{1}{2}}), \tag{1.13a}$$

from the given neighboring cell averages $\mathbf{U}_{i,j}, \mathbf{U}_{i\pm1,j}$ and $\mathbf{U}_{i,j}, \mathbf{U}_{i,j\pm1}$. The resulting second-order fluxes are then given by

$$\mathbf{F}_{i+\frac{1}{2},j} = \mathbf{F}(\mathbf{U}^E_{i,j}, \mathbf{U}^W_{i+1,j}), \quad \mathbf{G}_{i,j+\frac{1}{2}} = \mathbf{G}(\mathbf{U}^N_{i,j}, \mathbf{U}^S_{i,j+1}). \tag{1.13b}$$

The use of minmod limiter ensures the non-oscillatory behavior of the second-order schemes (1.6),(1.12). Observe that the second-order MUSCL fluxes (1.13b) are based on 4-point stencils

$$\mathbf{F}_{i+\frac{1}{2},j} = \mathbf{F}(\mathbf{U}_{i-1,j}, \mathbf{U}_{i,j}, \mathbf{U}_{i+1,j}, \mathbf{U}_{i+2,j}), \quad \mathbf{G}_{i,j+\frac{1}{2}} = \mathbf{F}(\mathbf{U}_{i,j-1}, \mathbf{U}_{i,j}, \mathbf{U}_{i,j+1}, \mathbf{U}_{i,j+2})$$

Similar reconstructions together with upwind or central averaging yield a large class of high-resolution finite-volume semi-discrete schemes, e.g., [23, 43, 24], which could then be integrated in time using standard stable high order Runge-Kutta methods [22].

1.2. **Genuinely multi-dimensional (GMD) fluxes.** Despite their considerable success, finite volume schemes (1.6) are known to be deficient in resolving genuinely multi-dimensional waves [26]. Observe that the numerical fluxes $\mathbf{F}_{i+\frac{1}{2},j}, \mathbf{G}_{i,j+\frac{1}{2}}$ in (1.11) are based on one-dimensional stencils which are supported in each normal direction but *lack explicit transverse information.* This could result in poor approximation of genuinely multi-dimensional waves, particularly for complicated systems like the ideal MHD equations (1.1). A characteristic feature of the MHD equations is the difference between the one- and multi-dimensional forms of (1.1) on account of the constraint. This aspect strongly illustrates the GMD nature of the MHD equations. Considerable effort has been devoted to devising *genuinely multi-dimensional* (GMD) finite volume schemes for approximating (1.1). The proposed methods include dimensional splitting [26], wave propagation algorithms [26, 27], method of transport [15, 16, 36], bi-characteristics based evolution Galerkin methods [28, 29] and fluctuation

splitting schemes [12]. However, there is a lack of an optimal strategy for designing GMD schemes for systems of conservation laws like the MHD equations.

This absence of an optimal strategy leaves room for designing stable GMD schemes that are easy to formulate and code, have a low computational cost and preserve other desirable properties rendered by the multi-dimensional structure of the system (1.1) like the divergence constraint. Their numerical fluxes take a general form

$$\mathbf{F}_{i+\frac{1}{2},j} = \mathbf{F}(\{\mathbf{U}_{(i',j')\in S_{i+\frac{1}{2},j}}\}), \quad \mathbf{G}_{i,j+\frac{1}{2}} = \mathbf{G}(\{\mathbf{U}_{(i',j')\in S_{i,j+\frac{1}{2}}}\}). \tag{1.14a}$$

Here, $S_{i+\frac{1}{2},j}$ and $S_{i,j+\frac{1}{2}}$ are *genuinely two-dimensional* stencils which, in contrast to (1.11), allow us to incorporate information from both the normal and transverse directions,

$$S_{i+\frac{1}{2},j} := \big\{(i',j') \,\big|\, |i'-i-1/2| + |j'-j| < q\big\}, \quad S_{i,j+\frac{1}{2}} := \big\{(i',j') \,\big|\, |i'-i| + |j'-j-1/2| < q\big\} \tag{1.14b}$$

We present such a family of GMD schemes in section 2, based on the GMD framework advocated in recent papers [31, 32].

1.3. **Divergence preserving schemes.** A major issue for the numerical approximation of multi-dimensional ideal MHD equations (1.1) is the divergence constraint (1.5). Standard finite volume schemes may not preserve discrete versions of the constraint, leading to numerical instabilities [47, 17]. Different approaches have been suggested to handle the divergence constraint in MHD codes and we mention three of the currently available approaches below.

1.4. **Projection method.** This method [10, 8, 6] is based on the Hodge decomposition of the solution $\mathbf{u}$ of (1.4). The update $\mathbf{u}^n$ at each time step may not be divergence free and is corrected by the decomposition, $\mathbf{u}^n = \nabla\Psi + \mathrm{curl}\Phi$. Applying the divergence operator to the Hodge decomposition leads to the elliptic equation:

$$-\Delta\Psi = \mathrm{div}(\mathbf{u}^n).$$

The corrected field $\mathbf{u}^* = \mathbf{u}^n - \nabla\Psi$ is divergence free. This method can be very expensive computationally as an elliptic equation has to be solved at every time step, augmented with proper set of boundary conditions, e.g. [47].

1.5. **Source terms.** Adding a source term proportional to the divergence in (1.4) results in

$$\mathbf{B}_t + \mathrm{curl}(\mathbf{B}\times\mathbf{u}) = -\mathbf{u}\mathrm{div}(\mathbf{B}). \tag{1.15}$$

Applying the divergence to both sides, we obtain

$$(\mathrm{div}\mathbf{B})_t + \mathrm{div}(\mathbf{u}\mathrm{div}\mathbf{B}) = 0.$$

Hence, any potential divergence errors are transported away from the computational domain by the flow. Furthermore, the form (1.15) is symmetrizable [38]. This procedure for "cleaning" the divergence was introduced in [38, 39]. Recent papers [17, 19] have demonstrated that the source term in (1.15) needs to be discretized in a very careful manner for numerical stability. Another problem with this approach lies in the non-conservative form of (1.15). Hence, numerical schemes based on this approach may result in wrong shock speeds [47]. A variant of this approach is the Generalized Lagrange multiplier method [13].

1.6. **Design of special divergence operators/staggering.** This popular method consists of staggering the discretizations of the velocity and magnetic fields in (1.4). A wide variety of strategies for staggering the meshes has been proposed [14, 5, 11, 42, 47, 3, 2] and references therein. The presence of different sets of meshes leads to problems when the staggered schemes are parallelized. Unstaggered variants of this approach have also been proposed in [45, 46, 1].

The above discussion suggests there is ample scope for a simple, computationally cheap finite volume scheme for the MHD equations that resolves genuinely multi-dimensional waves and preserves a discrete version of the divergence constraint. We design a method with these desired properties in this paper.

Our starting point are the *genuinely multi-dimensional* (GMD) finite volume schemes for systems of conservation laws proposed in recent papers [31, 32]. These schemes modify standard finite volume fluxes by introducing vertex centered *numerical potentials*. The potentials incorporate explicit transverse information and lead to

a stable and accurate resolution of genuinely multi-dimensional waves. A suitable choice of potentials results in GMD schemes that preserve constraints like divergence [31] and vorticity [32] in the magnetic induction equation and the system wave equation, respectively. The schemes are very simple to implement and have low computational cost.

We extend the GMD framework of [32] to the ideal MHD equations (1.1). The schemes are based on *numerical potentials*. A suitable choice of the potential leads to schemes that preserves discrete divergence. The rest of the paper is organized as follows: in section 2, we present the GMD framework of [32] and divergence preserving modifications are presented in section 3. Numerical experiments are reported in section 4.

2. Genuinely multi-dimensional (GMD) schemes

Following the presentation of [32], we introduce the *numerical potentials* $\phi_{i+\frac{1}{2},j+\frac{1}{2}}$ and $\psi_{i+\frac{1}{2},j+\frac{1}{2}}$ at each vertex $(x_{i+\frac{1}{2}}, y_{j+\frac{1}{2}})$, with the sole requirement that these potentials are consistent with the differential fluxes, i.e,

$$\phi_{i+\frac{1}{2},j+\frac{1}{2}}(\mathbf{U},\cdots,\mathbf{U}) = \mathbf{f}(\mathbf{U}), \quad \psi_{i+\frac{1}{2},j+\frac{1}{2}}(\mathbf{U},\cdots,\mathbf{U}) = \mathbf{g}(\mathbf{U}).$$

We need the following notation for standard averaging and (undivided) difference operators,

$$\begin{aligned} \mu_x a_{I,J} &:= \frac{a_{I+\frac{1}{2},J} + a_{I-\frac{1}{2},J}}{2}, \quad \mu_y a_{I,J} := \frac{a_{I,J+\frac{1}{2}} + a_{I,J-\frac{1}{2}}}{2}, \\ \delta_x a_{I,J} &:= a_{I+\frac{1}{2},J} - a_{I-\frac{1}{2},J}, \quad \delta_y a_{I,J} := a_{I,J+\frac{1}{2}} - a_{I,J-\frac{1}{2}}. \end{aligned} \tag{2.1}$$

A word about our notations: we note that the above discrete operators could be used with indexes I, J which are placed at the center or at the edge of the computational cells, e.g., $I = i$ or $I = i + \frac{1}{2}$. In either case, we tag the resulting discrete operators according to the center of their stencil; thus, for example, $\mu_x w_{i+\frac{1}{2}}$ employs grid values placed on the integer-indexed edges, w_i and w_{i+1}, whereas $\delta_y w_j$ employs the half-integer indexed centers, $w_{j\pm\frac{1}{2}}$.

We now set the numerical fluxes:

$$\begin{aligned} \mathbf{F}_{i+\frac{1}{2},j} &= \mu_y \phi_{i+\frac{1}{2},j}, \\ \mathbf{G}_{i,j+\frac{1}{2}} &= \mu_x \phi_{i,j+\frac{1}{2}}. \end{aligned} \tag{2.2}$$

The resulting finite volume scheme written in terms of the numerical potentials reads

$$\begin{aligned} \frac{d}{dt}\mathbf{U}_{i,j} &= -\frac{1}{\Delta x}\delta_x\mu_y\phi_{i,j} - \frac{1}{\Delta y}\delta_y\mu_x\psi_{i,j}, \\ &= -\frac{1}{\Delta x}\Big(\frac{1}{2}(\phi_{i+\frac{1}{2},j+\frac{1}{2}} + \phi_{i+\frac{1}{2},j-\frac{1}{2}}) - \frac{1}{2}(\phi_{i-\frac{1}{2},j+\frac{1}{2}} + \phi_{i-\frac{1}{2},j-\frac{1}{2}})\Big) \\ &\quad - \frac{1}{\Delta y}\Big(\frac{1}{2}(\psi_{i+\frac{1}{2},j+\frac{1}{2}} + \psi_{i-\frac{1}{2},j+\frac{1}{2}}) - \frac{1}{2}(\psi_{i+\frac{1}{2},j-\frac{1}{2}} + \psi_{i-\frac{1}{2},j-\frac{1}{2}})\Big). \end{aligned} \tag{2.3}$$

The potential based scheme (2.3) is clearly conservative as well as consistent as the potentials ϕ, ψ are consistent. The genuinely multi-dimensional nature of the scheme is evident from (2.3): the potentials are differenced in the normal direction but averaged in the transverse direction. We claim that the family of potential-based schemes (2.3) is *rich*: any standard finite volume flux can be used as a building block for constructing the numerical potentials in (2.2), and the resulting potential-based scheme inherits the accuracy of the underlying numerical flux. There are several ways to pursue the construction of numerical potentials and we outline three of them below.

2.1. Symmetric potentials.

In this approach, the potentials are defined by averaging the finite volume fluxes neighboring a vertex:

$$\begin{aligned} \phi_{i+\frac{1}{2},j+\frac{1}{2}} &= \mu_y \mathbf{F}_{i+\frac{1}{2},j+\frac{1}{2}}, \\ \psi_{i+\frac{1}{2},j+\frac{1}{2}} &= \mu_x \mathbf{G}_{i+\frac{1}{2},j+\frac{1}{2}}, \end{aligned} \tag{2.4}$$

where $\mathbf{F}, \mathbf{G}$ are any numerical fluxes consistent with $\mathbf{f}$ and $\mathbf{g}$ respectively. An explicit computation of (2.3) with potentials (2.4) leads to the revealing form,

$$\begin{aligned}\frac{d}{dt}\mathbf{U}_{i,j} = &-\frac{1}{2\Delta x}(\mu_y\mathbf{F}_{i+\frac{1}{2},j+\frac{1}{2}} + \mu_y\mathbf{F}_{i+\frac{1}{2},j-\frac{1}{2}} - \mu_y\mathbf{F}_{i-\frac{1}{2},j+\frac{1}{2}} - \mu_y\mathbf{F}_{i-\frac{1}{2},j-\frac{1}{2}})\\ &-\frac{1}{2\Delta y}(\mu_x\mathbf{G}_{i+\frac{1}{2},j+\frac{1}{2}} + \mu_x\mathbf{G}_{i-\frac{1}{2},j+\frac{1}{2}} - \mu_x\mathbf{G}_{i+\frac{1}{2},j-\frac{1}{2}} - \mu_x\mathbf{G}_{i-\frac{1}{2},j-\frac{1}{2}}).\end{aligned} \tag{2.5}$$

Comparing the potential based scheme (2.5) with the standard finite volume scheme (1.6), we observe that the potential based scheme modifies (1.6) by averaging the fluxes in the transverse direction. Hence, it incorporates *explicit* transverse information in each direction. When employing two-point fluxes, the local stencil for the GMD scheme (2.5) consists of nine points instead of the standard five point stencil for the finite volume scheme (1.6). One can use wider stencils to achieve higher-order of accuracy; for example, the symmetric potential-based scheme based on second-order four-point MUSCL flux (1.12) yields a second-order GMD scheme based on a stencil of twenty-three points.

2.2. **Weighted symmetric potentials.** Weighted averages of the neighboring fluxes can be considered in place of the simple averaging used in (2.4). For prescribed $\theta_{i+\frac{1}{2},j+\frac{1}{2}}, \kappa_{i+\frac{1}{2},j+\frac{1}{2}} \in (0,1)$, the weighted potential is defined as

$$\begin{aligned}\phi_{i+\frac{1}{2},j+\frac{1}{2}} &= \theta_{i+\frac{1}{2},j+\frac{1}{2}}\mathbf{F}_{i+\frac{1}{2},j+1} + (1-\theta_{i+\frac{1}{2},j+\frac{1}{2}})\mathbf{F}_{i+\frac{1}{2},j},\\ \psi_{i+\frac{1}{2},j+\frac{1}{2}} &= \kappa_{i+\frac{1}{2},j+\frac{1}{2}}\mathbf{G}_{i+1,j+\frac{1}{2}} + (1-\kappa_{i+\frac{1}{2},j+\frac{1}{2}})\mathbf{G}_{i,j+1/2}.\end{aligned} \tag{2.6}$$

The weights can be chosen based on the local characteristic speeds,

$$\begin{aligned}\theta_{i+\frac{1}{2},j+\frac{1}{2}} &= \frac{\max\{-(\beta_1)_{i+\frac{1}{2},j+\frac{1}{2}},0\}}{\max\{-(\beta_1)_{i+\frac{1}{2},j+\frac{1}{2}},0\} + \max\{(\beta_N)_{i+\frac{1}{2},j+\frac{1}{2}},0\}},\\ \kappa_{i+\frac{1}{2},j+\frac{1}{2}} &= \frac{\max\{-(\alpha_1)_{i+\frac{1}{2},j+\frac{1}{2}},0\}}{\max\{-(\alpha_1)_{i+\frac{1}{2},j+\frac{1}{2}},0\} + \max\{(\alpha_N)_{i+\frac{1}{2},j+\frac{1}{2}},0\}}.\end{aligned} \tag{2.7}$$

Here, α_l and , $\beta_l, l = 1, 2, \cdots, N$ are the real eigenvalues of $A = \partial_{\mathbf{U}}\mathbf{f}(\mu_y\mu_x\mathbf{U}_{i+\frac{1}{2},j+\frac{1}{2}})$ and $B = \partial_{\mathbf{U}}\mathbf{g}(\mu_x\mu_y\mathbf{U}_{i+\frac{1}{2},j+\frac{1}{2}})$, sorted in an increasing order. This choice of weights implies that the potential (2.6) is "upwinded".

2.3. **Diagonal potentials.** We define the diagonal potentials [31] ,

$$\begin{aligned}\phi_{i+\frac{1}{2},j+\frac{1}{2}} &= \frac{1}{2}\big(\mathbf{F}^+_{i+\frac{1}{2},j+\frac{1}{2}} + \mathbf{F}^-_{i+\frac{1}{2},j+\frac{1}{2}}\big),\\ \psi_{i+\frac{1}{2},j+\frac{1}{2}} &= \frac{1}{2}(\mathbf{G}^+_{i+\frac{1}{2},j+\frac{1}{2}} + \mathbf{G}^-_{i+\frac{1}{2},j+\frac{1}{2}}).\end{aligned} \tag{2.8a}$$

Here, $\mathbf{F}^\pm, \mathbf{G}^\pm$ are the *diagonal* fluxes

$$\begin{aligned}\mathbf{F}^+_{i+\frac{1}{2},j+\frac{1}{2}} &:= \mathbf{F}(\mathbf{U}_{i,j}, \mathbf{U}_{i+1,j+1}), \quad \mathbf{F}^-_{i+\frac{1}{2},j-\frac{1}{2}} = \mathbf{F}(\mathbf{U}_{i,j}, \mathbf{U}_{i+1,j-1})\\ \mathbf{G}^+_{i+\frac{1}{2},j+\frac{1}{2}} &:= \mathbf{G}(\mathbf{U}_{i,j}, \mathbf{U}_{i+1,j+1}), \quad \mathbf{G}^-_{i-\frac{1}{2},j+\frac{1}{2}} := \mathbf{G}(\mathbf{U}_{i,j}, \mathbf{U}_{i-1,j+1}).\end{aligned} \tag{2.8b}$$

which amount to rotating the x- and y-axis by angles of $\frac{\pi}{4}$ and $-\frac{\pi}{4}$, where $\mathbf{F}(\cdot,\cdot)$ and $\mathbf{G}(\cdot,\cdot)$ are any two-point numerical fluxes consistent with $\mathbf{f}$ and $\mathbf{g}$.

2.4. **Isotropic GMD scheme.** We conclude our list for recipes of GMD schemes with an example which is *not* rendered by a numerical potential, but nevertheless, highlights the use of a GMD stencil. Let $\mathbf{F}(\cdot,\cdot)$ and $\mathbf{G}(\cdot,\cdot)$ are any two-point consistent numerical fluxes and let $\mathbf{F}^\pm, \mathbf{G}^\pm$ be the corresponding diagonal numerical fluxes in (2.8b). We define the isotropic fluxes,

$$\begin{aligned}\widetilde{F}_{i+\frac{1}{2},j} &:= \frac{1}{4}\big(\mathbf{F}^+_{i+\frac{1}{2},j+\frac{1}{2}} + 2\mathbf{F}_{i+\frac{1}{2},j} + \mathbf{F}^-_{i+\frac{1}{2},j-\frac{1}{2}}\big),\\ \widetilde{G}_{i,j+\frac{1}{2}} &:= \frac{1}{4}\big(\mathbf{G}^+_{i+\frac{1}{2},j+\frac{1}{2}} + 2\mathbf{G}_{i,j+\frac{1}{2}} + \mathbf{G}^-_{i-\frac{1}{2},j+\frac{1}{2}}\big).\end{aligned} \tag{2.9a}$$

The resulting finite volume scheme reads as

$$\begin{aligned}\frac{d}{dt}\mathbf{U}_{i,j} &= -\frac{1}{\Delta x}\delta_x\widetilde{\mathbf{F}}_{i,j} - \frac{1}{Dy}\delta_y\widetilde{\mathbf{G}}_{i,j},\\ &= -\frac{1}{4\Delta x}\left(\delta_/\mathbf{F}^+_{i,j} + 2\delta_x\mathbf{F}_{i,j} + \delta_\backslash F^-_{i,j}\right) - \frac{1}{4\Delta y}\left(\delta_/\mathbf{G}^+_{i,j} + 2\delta_y\mathbf{G}_{i,j} - \delta_\backslash G^-_{i,j}\right);\end{aligned} \tag{2.9b}$$

here, $\delta_/$ and $\delta_\backslash$ denote the *diagonal* difference operators,

$$\delta_/ a_{I,J} := a_{I+\frac{1}{2},J+\frac{1}{2}} - a_{I-\frac{1}{2},J-\frac{1}{2}}, \quad \delta_\backslash a_{I,J} := a_{I+\frac{1}{2},J-\frac{1}{2}} - a_{I-\frac{1}{2},J+\frac{1}{2}}. \tag{2.10}$$

The GMD structure of the scheme is clear from (2.9b): the scheme averages the fluxes along transverse directions. In contrast to the symmetric scheme (2.5), however, the explicit transverse information in (2.9b) is obtained by "rotating" the fluxes. Since the scheme (2.9b) takes into account all the directions in a cell, we term it as the *isotropic* GMD scheme.

The isotropic GMD scheme (2.9b) is a desirable form of GMD schemes as it is shown to be entropy stable, see [32].

The stencil of the isotropic scheme consists of nine points. Second-order accuracy can be obtained by the piecewise bilinear reconstruction (1.12). In addition to (1.13), we also need the corner point values,

$$\begin{aligned}\mathbf{U}^{NE}_{i,j} &:= \mathbf{p}_{i,j}(x_{i+\frac{1}{2}}, y_{j+\frac{1}{2}}), \quad \mathbf{U}^{NW}_{i,j} := \mathbf{p}_{i,j}(x_{i-\frac{1}{2}}, y_{j+\frac{1}{2}}),\\ \mathbf{U}^{SE}_{i,j} &:= \mathbf{p}_{i,j}(x_{i+\frac{1}{2}}, y_{j-\frac{1}{2}}), \quad \mathbf{U}^{SW}_{i,j} := \mathbf{p}_{i,j}(x_{i-\frac{1}{2}}, y_{j-\frac{1}{2}}),\end{aligned} \tag{2.11a}$$

and the corresponding diagonal fluxes,

$$\begin{aligned}\mathbf{F}^+_{i+\frac{1}{2},j+\frac{1}{2}} &:= \mathbf{F}(\mathbf{U}^{NE}_{i,j}, \mathbf{U}^{SW}_{i+1,j+1}), \quad \mathbf{F}^-_{i+\frac{1}{2},j-\frac{1}{2}} := \mathbf{F}(\mathbf{U}^{SE}_{i,j}, \mathbf{U}^{NW}_{i+1,j+1}),\\ \mathbf{G}^+_{i+\frac{1}{2},j+\frac{1}{2}} &:= \mathbf{G}(\mathbf{U}^{NE}_{i,j}, \mathbf{U}^{SW}_{i+1,j+1}), \quad \mathbf{G}^-_{i-\frac{1}{2},j+\frac{1}{2}} := \mathbf{F}(\mathbf{U}^{NW}_{i,j}, \mathbf{U}^{SE}_{i-1,j+1}),\end{aligned} \tag{2.11b}$$

to define the second order accurate version of the isotropic GMD scheme.

3. Divergence preserving schemes

The divergence of the magnetic field in (1.1) is preserved (1.5). Despite incorporating transverse information, the GMD schemes (2.5) and (2.9) may not necessarily preserve a discrete version of the divergence constraint. A possible explanation lies in the special structure of the fluxes $\mathbf{f}$ and $\mathbf{g}$ in (1.1).

The 8-vectors of fluxes associated with the ideal MHD equations (1.1) satisfy,

$$\mathbf{f}_5 = \mathbf{g}_6 \equiv 0, \quad -\mathbf{f}_6 = \mathbf{g}_5 = u_2B_1 - u_1B_2. \tag{3.1}$$

This structure of the fluxes ensures that the divergence is preserved. Accordingly, we need to respect this special structure at the discrete level by choosing a suitable form of the potential to ensure a divergence-free numerical solution. This is done by choosing numerical potentials,

$$\begin{aligned}\phi_{i+\frac{1}{2},j+\frac{1}{2}} &= \{(\phi_1)_{i+\frac{1}{2},j+\frac{1}{2}}, \cdots, (\phi_4)_{i+\frac{1}{2},j+\frac{1}{2}}, 0, -\chi_{i+\frac{1}{2},j+\frac{1}{2}}, (\phi_7)_{i+\frac{1}{2},j+\frac{1}{2}}, (\phi_8)_{i+\frac{1}{2},j+\frac{1}{2}}\},\\ \psi_{i+\frac{1}{2},j+\frac{1}{2}} &= \{(\psi_1)_{i+\frac{1}{2},j+\frac{1}{2}}, \cdots, (\psi_4)_{i+\frac{1}{2},j+\frac{1}{2}}, \chi_{i+\frac{1}{2},j+\frac{1}{2}}, 0, (\psi_7)_{i+\frac{1}{2},j+\frac{1}{2}}, (\psi_8)_{i+\frac{1}{2},j+\frac{1}{2}}\}.\end{aligned} \tag{3.2}$$

Here

$$\eta = (\phi_1, \cdots, \phi_4, \phi_7, \phi_8), \quad \zeta = (\psi_1, \cdots, \psi_4, \psi_7, \psi_8)$$

are the corresponding components of any consistent potentials ϕ and ψ respectively.

The remaining non-zero component of the potentials (3.2), χ needs to be consistent with $-\mathbf{f}_6 = \mathbf{g}_5 = u_1B_2 - u_2B_1$. Introducing

$$\mathbf{V} = \{\rho, \rho u_1, \rho u_2, \rho u_3, B_3, E\},$$

the divergence preserving version of the potential based scheme (2.3) reads as

$$\begin{aligned}\frac{d}{dt}\mathbf{V}_{i,j} &= -\frac{1}{\Delta x}\delta_x\mu_y\eta_{i,j} - \frac{1}{\Delta y}\delta_y\mu_x\zeta_{i,j},\\ \frac{d}{dt}(B_1)_{i,j} &= -\frac{1}{\Delta y}\delta_y\mu_x\chi_{i,j},\\ \frac{d}{dt}(B_2)_{i,j} &= \frac{1}{\Delta x}\delta_x\mu_y\chi_{i,j}.\end{aligned} \tag{3.3}$$

The above scheme amounts to a specific form of the potential based scheme (2.3). Its divergence preserving property is summarized below.

Lemma 3.1. *Let* $\mathbf{B}_{i,j}$ *be the approximate magnetic fields for* (1.1) *computed with* (3.3)*. Then their discrete divergence* div^**, given by*

$$\mathrm{div}^*_{i,j} = \frac{1}{\Delta x}\mu_y\delta_x(B_1)_{i,j} + \frac{1}{\Delta y}\mu_x\delta_y(B_2)_{i,j}, \tag{3.4a}$$

is preserved in time, i.e,

$$\frac{d}{dt}(\mathrm{div}^*_{i,j}) \equiv 0, \quad \forall i,j. \tag{3.4b}$$

The verification of (3.4b) is straightforward as the difference operators δ_x, δ_y and the averaging operators μ_x, μ_y commute with each other. We apply the discrete divergence operator div^* to the numerical scheme (3.3) to find

$$\Delta x\Delta y\frac{d}{dt}\mathrm{div}^*_{i,j} = (\mu_x\delta_y\delta_x\mu_y - \mu_y\delta_x\delta_x\mu_x)\chi_{i,j} \equiv 0.$$

Remark 3.1. *One approach in designing constraint preserving schemes is to satisfy that constraint* approximately*: for example, the discrete statement of the divergence constraint could be interpreted as a second-order approximation of the differential divergence ,*

$$\mathrm{div}^*_{i,j} = \mathrm{div}(x_i, y_j) + \mathcal{O}(\Delta x^2 + \Delta y^2).$$

This, however, requires the smoothness of the underlying solution. Instead, a key feature of constraint preserving schemes based on numerical potentials is that they satisfy exactly *a discrete constraint, so that their numerical solution remains on a discrete sub-manifold, independent of the underlying smoothness. Similarly, a related potential-based GMD scheme which preserves a discrete vorticity was described in* [32].

The scalar potential χ in (3.3) can be chosen in different ways. We mention two possible choices below.

3.1. **Divergence preserving symmetric GMD scheme.** The potentials η, ζ are defined as in (2.4). A natural choice [31] of the potential χ is the symmetric potential:

$$\chi_{i+\frac{1}{2},j+\frac{1}{2}} = \frac{1}{4}((\mathbf{F}_6)_{i+\frac{1}{2},j} + (\mathbf{F}_6)_{i+\frac{1}{2},j+1} + (\mathbf{G}_5)_{i,j+\frac{1}{2}} + (\mathbf{G}_5)_{i+1,j+\frac{1}{2}}) \tag{3.5}$$

with $\mathbf{F}_{5,6}, \mathbf{G}_{5,6}$ being components of any consistent numerical fluxes $\mathbf{F}, \mathbf{G}$. Let

$$\mathbf{H} = \{\mathbf{F}_1, \cdots, \mathbf{F}_4, \mathbf{F}_7, \mathbf{F}_8\}, \quad \mathbf{K} = \{\mathbf{G}_1, \cdots, \mathbf{G}_4, \mathbf{G}_7, \mathbf{G}_8\}$$

for any consistent fluxes $\mathbf{F}, \mathbf{G}$. The divergence preserving symmetric GMD scheme has the explicit form:

$$\begin{aligned}\frac{d}{dt}\mathbf{V}_{i,j} &= -\frac{1}{2\Delta x}(\mu_y\mathbf{H}_{i+\frac{1}{2},j+\frac{1}{2}} + \mu_y\mathbf{H}_{i+\frac{1}{2},j-\frac{1}{2}} - \mu_y\mathbf{H}_{i-\frac{1}{2},j+\frac{1}{2}} - \mu_y\mathbf{H}_{i-\frac{1}{2},j-\frac{1}{2}})\\ &\quad - \frac{1}{2\Delta y}(\mu_x\mathbf{K}_{i+\frac{1}{2},j+\frac{1}{2}} + \mu_x\mathbf{K}_{i-\frac{1}{2},j+\frac{1}{2}} - \mu_x\mathbf{K}_{i+\frac{1}{2},j-\frac{1}{2}} - \mu_x\mathbf{K}_{i-\frac{1}{2},j-\frac{1}{2}}),\\ \frac{d}{dt}(B_1)_{i,j} &= -\frac{1}{4\Delta y}(\mu_x(\mathbf{F}_6)_{i,j+1} - \mu_x(\mathbf{F}_6)_{i,j-1}) - \frac{1}{4\Delta y}(\delta_y(\mu_x(\mathbf{G}_5)_{i+\frac{1}{2},j+\frac{1}{2}} + \mu_x(\mathbf{G}_5)_{i-\frac{1}{2},j+\frac{1}{2}})),\\ \frac{d}{dt}(B_2)_{i,j} &= \frac{1}{4\Delta x}(\mu_y(\mathbf{G}_5)_{i+1,j} - \mu_y(\mathbf{G}_5)_{i-1,j}) + \frac{1}{4\Delta x}(\delta_x(\mu_y(\mathbf{F}_6)_{i+\frac{1}{2},j+\frac{1}{2}} + \mu_y(\mathbf{F}_6)_{i+\frac{1}{2},j-\frac{1}{2}})).\end{aligned} \tag{3.6}$$

3.2. **Divergence preserving isotropic GMD scheme.** We define a *diagonal* form of the potential χ:

$$\chi_{i+\frac{1}{2},j+\frac{1}{2}} = \frac{1}{4}((\mathbf{F}_6^+)_{i+\frac{1}{2},j+\frac{1}{2}} + (\mathbf{G}_5^+)_{i+\frac{1}{2},j+\frac{1}{2}} + (\mathbf{F}_6^-)_{i+\frac{1}{2},j+\frac{1}{2}} + (\mathbf{G}_5^-)_{i+\frac{1}{2},j+\frac{1}{2}}) \tag{3.7}$$

for diagonal fluxes $\mathbf{F}^\pm, \mathbf{G}^\pm$ defined in (2.8b). Denote

$$\mathbf{H}^\pm = \{\mathbf{F}_1^\pm, \cdots, \mathbf{F}_4^\pm, \mathbf{F}_7^\pm, \mathbf{F}_8^\pm\}, \quad \mathbf{K}^\pm = \{\mathbf{G}_1^\pm, \cdots, \mathbf{G}_4^\pm, \mathbf{G}_7^\pm, \mathbf{G}_8^\pm\}$$

The divergence preserving modification of the isotropic GMD scheme (2.9) based on the potential (3.7) is

$$\begin{aligned}
\frac{d}{dt}\mathbf{V}_{i,j} &= -\frac{1}{4\Delta x}\left(\delta_/\mathbf{H}_{i,j}^+ + 2\delta_x\mathbf{H}_{i,j} + \delta_\backslash\mathbf{H}_{i,j}^-\right) - \frac{1}{4\Delta y}\left(\delta_/\mathbf{K}_{i,j}^+ + 2\delta_y\mathbf{K}_{i,j} - \delta_\backslash\mathbf{K}_{i,j}^-\right), \\
\frac{d}{dt}(B_1)_{i,j} &= -\frac{1}{4\Delta y}\left(\mu_x\delta_y((\mathbf{F}_6^+)_{i,j} + (\mathbf{F}_6^-)_{i,j} + (\mathbf{G}_5^+)_{i,j} + (\mathbf{G}_5^-)_{i,j})\right), \\
\frac{d}{dt}(B_2)_{i,j} &= \frac{1}{4\Delta x}\left(\mu_y\delta_x((\mathbf{F}_6^+)_{i,j} + (\mathbf{F}_6^-)_{i,j} + (\mathbf{G}_5^+)_{i,j} + (\mathbf{G}_5^-)_{i,j})\right).
\end{aligned} \tag{3.8}$$

4. Numerical Results

All the potential based GMD schemes described in the previous section are semi-discrete. We define a fully discrete version of the first-order GMD schemes by using standard forward Euler time integration. Second-order strong stability preserving Runge-Kutta method [22] defines fully discrete versions of the second-order accurate GMD schemes. The time step is determined by a standard CFL condition. A CFL number of 0.45 is used in all the subsequent simulations.

We test the following schemes:

SYM (SYM2)	First (second)-order version of the symmetric GMD scheme (2.5).
ISO (ISO2)	First (second)-order version of the isotropic GMD scheme (2.9).
SCP (SCP2)	First (second)-order version of the divergence preserving symmetric GMD scheme (3.6).
ICP (ICP2)	First (second)-order version of the divergence preserving isotropic GMD scheme (3.8).

4.1. **Orszag-Tang vortex.** The Orszag-Tang vortex is a widely reported benchmark for multi-dimensional MHD equations [47]. The initial data is

$$(\rho, u_1, u_2, u_3, B_1, B_2, B_3, p) = \left(\gamma^2, -\sin(y), \sin(x), 0, -\sin(y), \sin(2x), 0, \gamma\right),$$

in the computational domain: $(x, y, t) \in [0, 2\pi]^2 \times [0, \pi]$ with periodic boundary conditions.

Although the exact solution is not known, qualitative features have been reported [47]. The solution consists of shocks along the diagonals and interesting smooth features including a vortex near the center of the domain. The approximate pressures, computed on a 200×200 mesh, are shown in figures 1 and 2.

Figure 1 shows the approximate pressure computed with the first-order GMD schemes. The solution is smeared at this resolution, but the qualitative features are captured without any spurious oscillations and other numerical artifacts. The divergence preserving SCP and ICP schemes are clearly more accurate than the SYM and ISO schemes, indicating that preserving a discrete version of the constraint leads to a gain in accuracy. The results for the second-order schemes are plotted in figure 2 and show a *considerable* improvement in the resolution. The gain in accuracy is pronounced, both at the shocks and at the central vortex. The divergence preserving SCP2 and ICP2 are slightly more accurate than the SYM2 and ISO2 schemes.

In the absence of an exact formula for the solution, the maximum pressure [47, 17] has been suggested as a measure of accuracy. The maximum pressure at time $t = \pi$, computed on a sequence of meshes, is presented in Table 1. The table provides a quantitative comparison between the schemes and vindicates the conclusions from the plots. The first-order schemes are diffusive, with a consistent gain in accuracy when the divergence preserving SCP and ICP schemes are used. The gain in resolution with the second-order schemes is considerable.

As the initial data is divergence free, the divergence constraint (1.5) implies that the divergence should remain zero during the evolution. We show the errors in the discrete divergence operator div^* (3.4a), measured in the L^1 norm, in Table 2. The table shows that the standard GMD schemes lead to $\mathcal{O}(1)$ divergence errors. Large

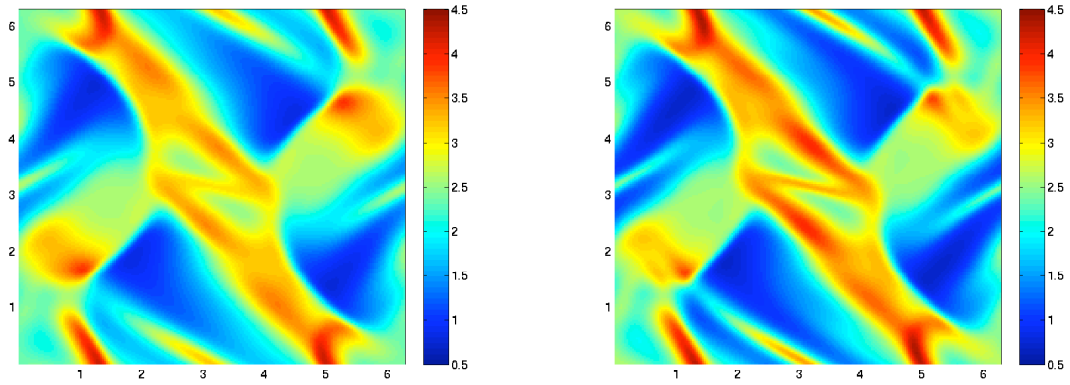

(a) SYM

(b) SCP

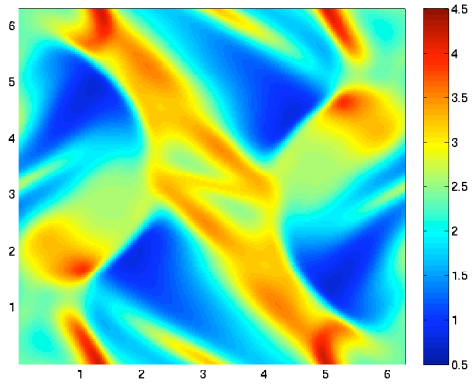

(c) ISO

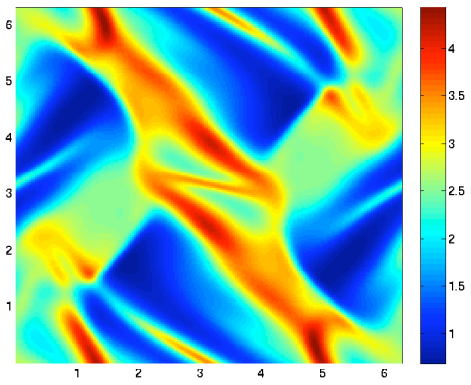

(d) ICP

FIGURE 1. The pressure p for the Orszag-Tang vortex computed at $t = \pi$ on a 200×200 mesh with first-order GMD schemes.

M	SYM	ISO	SCP	ICP	SYM2	ISO2	SCP2	ICP2
50	3.17	3.19	3.27	3.32	4.85	4.34	4.89	4.37
100	3.54	3.57	3.65	3.71	4.91	5.00	5.1	5.14
200	4.24	4.22	4.37	4.42	5.75	5.64	5.76	5.71
400	4.78	4.79	4.94	5.00	6.03	6.1	6.08	6.15

TABLE 1. Maximum pressure for the Orszag-Tang vortex with all the GMD schemes on a $M \times M$ mesh at time $t = \pi$.

M	SYM	ISO	SCP	ICP	SYM2	ISO2	SCP2	ICP2
50	0.53	0.42	4.7e-12	4.4e-12	1.49	1.32	5.8e-13	3.4e-13
100	0.89	0.70	2.1e-12	1.7e-12	3.39	3.07	5.1e-13	3.8e-13
200	1.23	1.11	1.0e-12	6.9e-13	5.57	5.12	5.7e-13	3.0e-13
400	1.61	1.52	1.3e-12	6.0e-13	8.08	11.3	6.0e-13	3.1e-13

TABLE 2. Discrete divergence div^* (3.4a) in L^1 for the Orszag-Tang vortex with all the GMD schemes on a $M \times M$ mesh at time $t = \pi$.

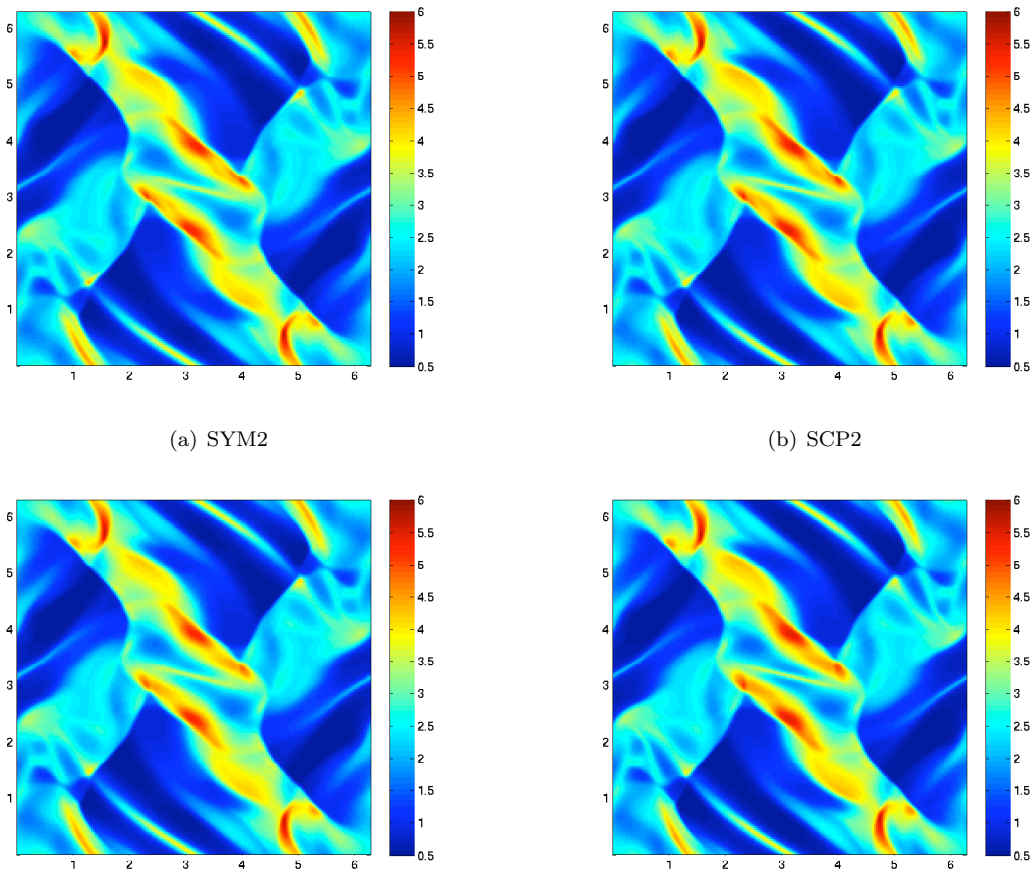

(a) SYM2 (b) SCP2

(c) ISO2 (d) ICP2

FIGURE 2. The pressure p for the Orszag-Tang vortex computed at $t = \pi$ on a 200×200 mesh with second-order GMD schemes.

amounts of discrete divergence is generated near the shocks. The divergence error is larger for the second-order SYM2 and ISO2 schemes than the first-order schemes. This is to be expected as the second-order schemes resolve the shocks sharply. On the other hand the SCP, SCP2, ICP and ICP2 schemes preserve the discrete divergence to machine precision.

Tables 1 and 2 show that the all the GMD schemes (whether they preserve a discrete version of divergence or not) are stable and do not crash at these resolutions. Note that numerical stability (particularly on fine meshes) for the MHD equations is delicate [17]. Standard schemes (even those with some form divergence cleaning) may crash due to instabilities and negative pressures on fine resolutions [17]. In spite of the large divergence errors, the SYM (SYM2) and ISO (ISO2) schemes are stable.

4.2. **Rotor problem.** Another benchmark test for the MHD equations is the rotor problem [47]. The computational domain is $(x, y, t) \in [0, 1]^2 \times [0, 0.295]$ with artificial Neumann type boundary conditions. The initial density is

$$\rho = \begin{cases} 10.0 & \text{if } r < 0.1, \\ 1 + 9f(r) & \text{if } 0.1 \le r < 0.115, \\ 1.0 & \text{otherwise,} \end{cases}$$

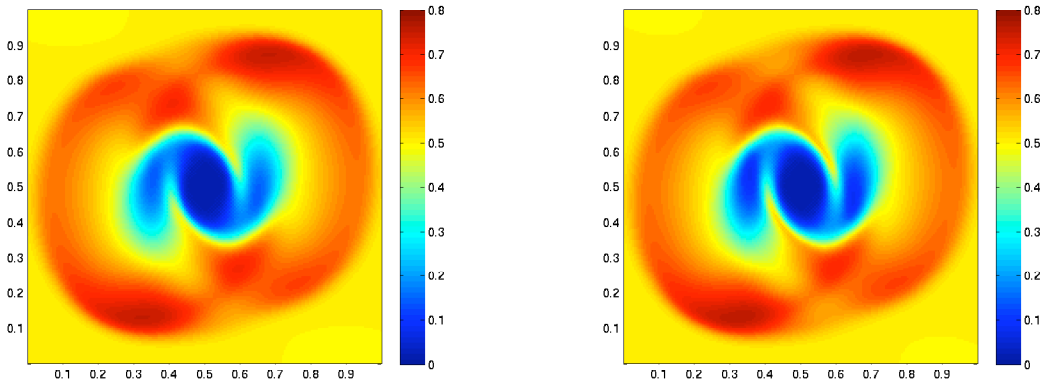

(a) SYM

(b) ISO

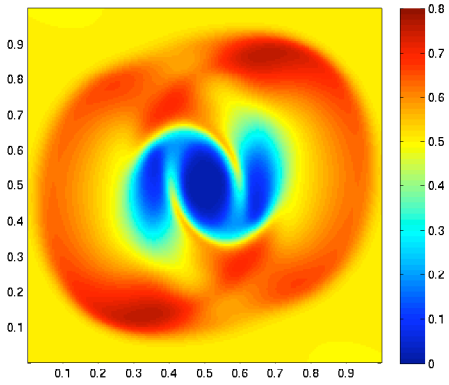

(c) SCP

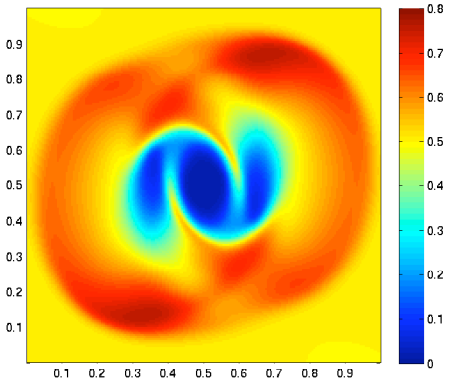

(d) ICP

FIGURE 3. The pressure p for the rotor problem computed at $t = 0.295$ on a 200×200 mesh with first-order schemes.

with $r(x, y) = |(x, y) - (0.5, 0.5)|$ and

$$f(r) = \frac{23 - 200r}{3}.$$

The other variables are initially,

$$(\rho u_1, \rho u_2) = \begin{cases} ((10y - 5)\rho, -(10x - 5)\rho) & \text{if } r < 0.1, \\ ((10y - 5)f(r)\rho, -(10x - 5)f(r)\rho) & \text{if } 0.1 \leq r < 0.115, \\ (0.0, 0.0) & \text{otherwise,} \end{cases}$$

$$(\rho u_3, B_1, B_2, B_3, p) = \left(0.0, 2.5/\sqrt{\pi}, 0.0, 0.0, 0.5\right).$$

The initial velocity and magnetic fields are such that the variables are rotated in the domain. The pressure drops to very low values in the center, and this test case is set up in order to determine how a scheme handles low pressures. The approximate pressure computed with the first-order GMD schemes, on a 200×200 mesh, is shown in figure 3. The figure shows that all the schemes are stable at this resolution and the low pressure at the center is resolved. The first-order schemes are diffusive, particularly at the shocks. The divergence preserving SCP and ICP schemes are more accurate in this case. The results for the second-order schemes are plotted in figure 4. They reveal a significant gain in resolution with the second-order schemes, particularly at shocks.

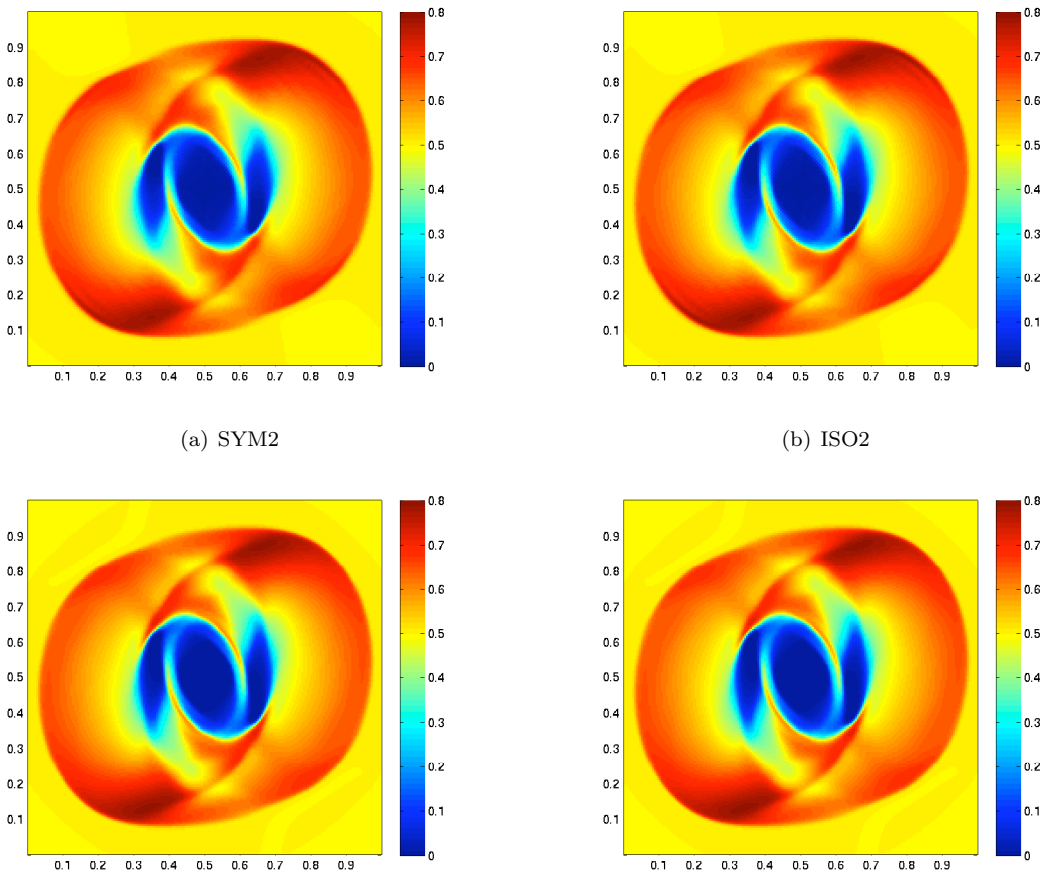

(a) SYM2 (b) ISO2

(c) SCP2 (d) ICP2

FIGURE 4. The pressure p for the rotor problem computed at $t = 0.295$ on a 200×200 mesh with second-order schemes.

The errors in the discrete divergence div^* are displayed in Table 3. The divergence errors generated by the SYM and ISO schemes and their second-order versions are again $\mathcal{O}(1)$. These errors increase with increasing resolution, i.e, either by reducing mesh size or by increasing the order of accuracy of the scheme, indicating that the bulk of the divergence errors are generated near the shocks. The SCP, ICP, SCP2 and ICP2 schemes preserve discrete divergence to machine precision.

4.3. **Cloud-Shock Interaction.** Another benchmark test case for the MHD equations involves the interaction of a high density cloud with a shock. The initial data for this cloud-shock interaction problem [41] consists of a shock located at $x = 0.05$ with

$$(\rho, u_1, u_2, u_3, B_1, B_2, B_3, p) = \begin{cases} (3.86859, 11.2536, 0, 0, 0, 2.1826182, -2.1826182, 167.345), & \text{if } x < 0.05 \\ (1.0, 0, 0, 0, 0, 0.56418958, 0.56418958, 1.0), & \text{if } x < 0.05. \end{cases} \tag{4.1}$$

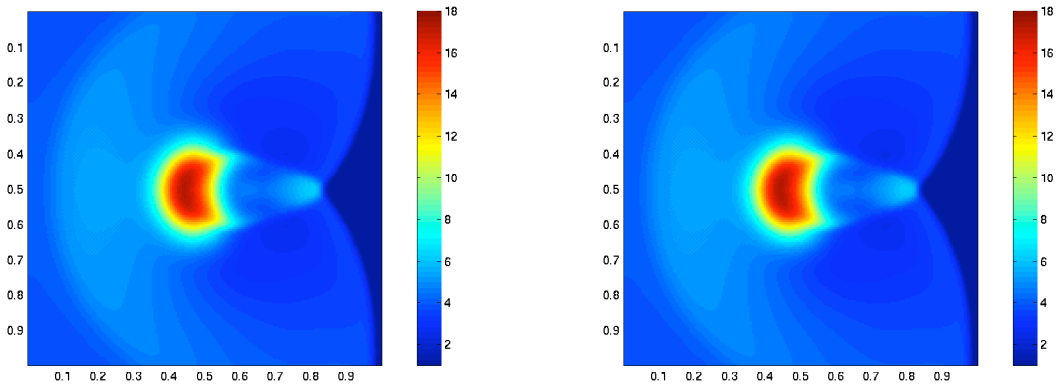

(a) SYM

(b) ISO

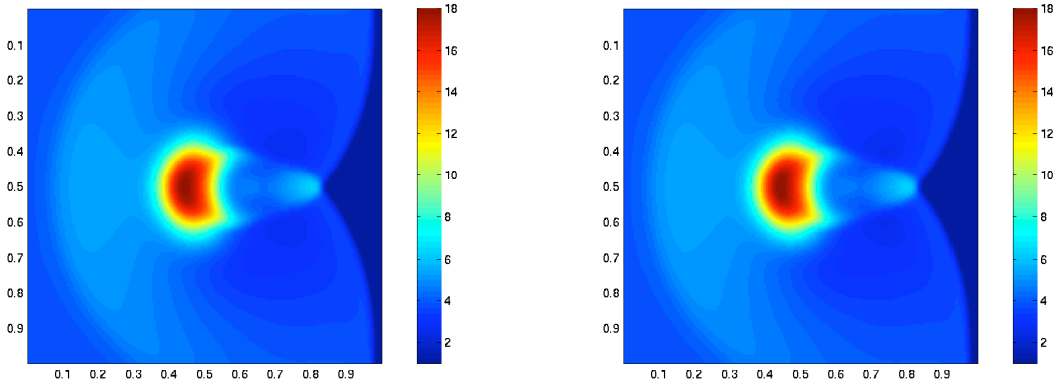

(c) SCP

(d) ICP

FIGURE 5. The density ρ for the cloud-shock interaction computed at $t = 0.06$ on a 200×200 mesh with first-order schemes.

and a circular cloud of density $\rho = 10$ with radius 0.15, centered at $(x, y) = (0.25, 0.5)$. The computational domain is $[0, 1] \times [0, 1]$. The test is configured in such a way that a right moving shock violently interacts with a high density cloud. The solution has a extremely complex structure, consisting of bow shock at the left, trailing shocks at the right and a complicated smooth region with turbulent features in the center.

M	SYM	ISO	SCP	ICP	SYM2	ISO2	SCP2	ICP2
50	0.70	0.57	6.0e-12	4.49e-12	1.03	1.03	6.3e-13	4.7e-13
100	1.25	0.93	2.3e-12	1.73e-12	1.92	1.9	2.4e-13	1.8e-13
200	1.7	1.23	8.8e-13	6.35e-13	3.41	3.27	4.1e-13	1.6e-13
400	2.09	1.56	3.3e-13	2.49e-13	6.0	5.7	4.2e-13	1.1e-13

TABLE 3. Discrete divergence div^* (3.4a) in L^1 for the rotor problem with all the eight schemes on a $M \times M$ mesh at time $t = 0.295$.

We plot the approximate density, on a 200×200 mesh , at time $t = 0.06$ in figures 5 and 6.

The first-order results in figure 5 show that the first-order GMD schemes are stable but quite diffusive. The divergence preserving SCP and ICP schemes are again more accurate than the SYM and ISO schemes. The

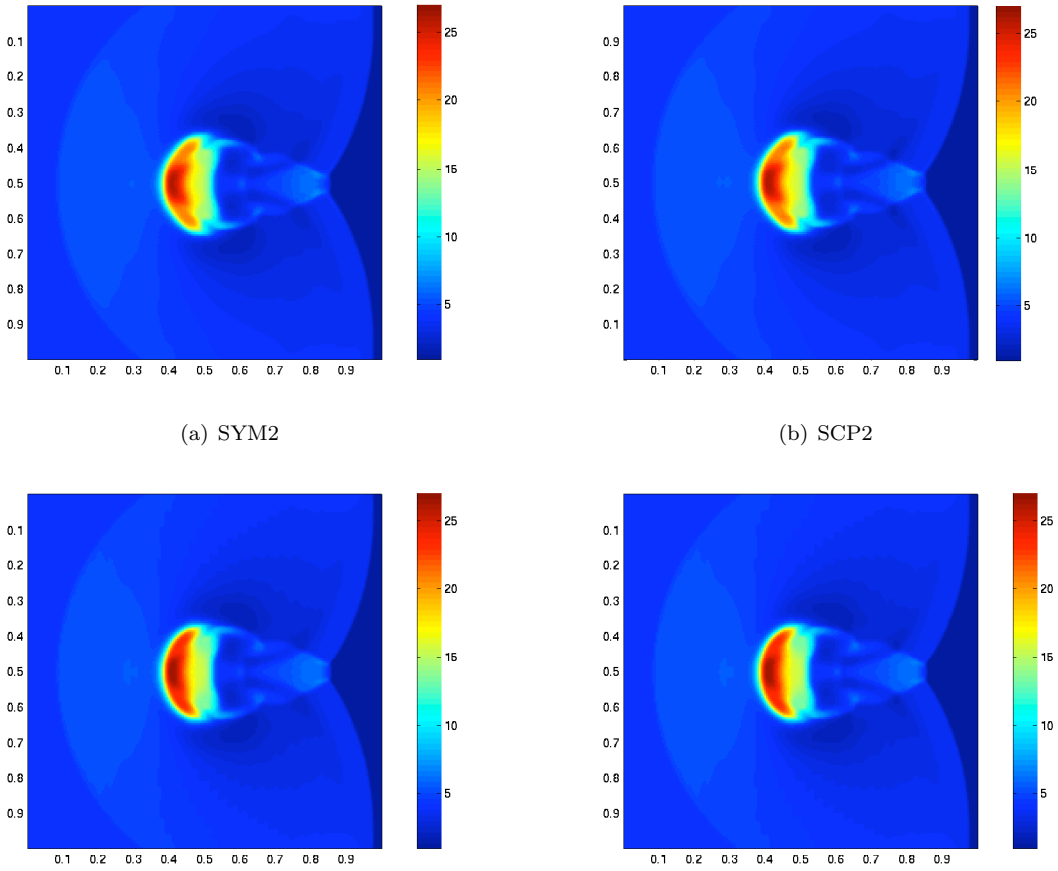

(a) SYM2 (b) SCP2

(c) ISO2 (d) ICP2

FIGURE 6. The density ρ for the cloud-shock interaction computed at $t = 0.06$ on a 200×200 mesh with second-order schemes

second-order results are plotted in figure 6 and show a *dramatic* increase in resolution with the second-order schemes. Both the bow shock and the trailing shock are captured accurately. The smooth region with turbulent like features is also resolved quite well. The divergence errors for discrete divergence div^* are shown in Table 4. The table shows large divergence errors for the SYM (SYM2) and ISO (ISO2) schemes. On the other hand, the constraint preserving SCP (SCP2) and ICP (ICP2) schemes preserve discrete divergence to machine precision.

M	SYM	ISO	SCP	ICP	SYM2	ISO2	SCP2	ICP2
50	4.56	2.59	2.8e-12	2.1e-12	5.79	5.38	3.4e-13	2.27e-13
100	4.47	3.3	1.2e-12	8.7e-13	12.58	11.75	2.1e-13	1.14e-13
200	5.19	4.05	5.0e-13	3.7e-13	27.1	26.48	1.4e-13	1.34e-13
400	7.5	6.4	2.3e-13	1.5e-13	38.0	41.3	1.8e-13	2.2e-13

TABLE 4. Discrete divergence div^* (3.4a) in L^1 for cloud shock interaction with all the eight schemes on a $M \times M$ mesh at time $t = 0.06$.

Remark 4.1. *The first-order GMD schemes were quite diffusive. A possible reason is the use of the Rusanov flux* (1.8)*. This flux is known to produce excessive smearing at the shocks. However, we advocate the use of the*

Rusanov flux as the accuracy is recovered at second-order. The Rusanov flux is very easy to implement, uses minimal characteristic information and has a low computational cost. It fits into the black box framework of our GMD schemes.

The three numerical experiments show that the GMD schemes are quite robust. There does not appear to be a strong connection between the divergence errors and stability of a GMD scheme. The GMD structure of the schemes incorporates stability. However, there is a gain in accuracy (at least at first-order) when the divergence preserving versions of the scheme are used.

Physicists are generally reluctant to use numerical schemes that produce divergence errors. Hence, we advocate the use of the divergence preserving GMD schemes. Furthermore, the computational cost of a divergence preserving GMD scheme is virtually identical to the cost of other GMD schemes.

5. Conclusion

The ideal MHD equations (1.1) are considered. The equations are non-strictly hyperbolic and posses a complex shock structure. Design of stable and accurate numerical methods for the MHD equations in multi-dimensions is complicated on account of its genuinely multi-dimensional structure and the divergence constraint.

We extend the potential based GMD framework of recent papers [31, 32] to the MHD equations. The finite volume schemes are formulated in terms of vertex centered *numerical potentials*. Symmetric (2.5) and isotropic (2.9) versions of the potential based GMD schemes are described. The GMD schemes are modified with a suitable choice of potentials to yield divergence preserving GMD schemes. Second-order versions are obtained by employing non-oscillatory piecewise bilinear reconstructions. The schemes are constraint preserving GMD extensions of the central schemes of Kurganov and Tadmor [24].

Benchmark numerical experiments for the MHD equations are presented. They show that the first-order GMD schemes resolve the waves with some diffusion. There is a gain in accuracy when the divergence preserving versions are used. The gain in resolution with the second-order schemes is considerable. The multi-dimensional shocks are vortices are captured, with good accuracy.

The *non divergence preserving* versions of the GMD schemes can generate large divergence errors, particularly at shocks. These errors do not seem to affect the stability of the schemes, at least in our tests. But large divergence errors might create instabilities at finer resolutions. Hence, we advocate using the divergence preserving versions of the GMD schemes. The GMD approach is simple to implement, robust and has a very low computational cost. It will be extended to higher than second-order of accuracy and to unstructured meshes in future papers. Other future projects include using the divergence preserving GMD schemes to compute realistic flows in solar physics and astrophysics.

References

[1] R. Artebrant and M.Torrilhon. Increasing the accuracy of local divergence preserving schemes for MHD. *J. Comp. Phys.*, 227 (6), 3405-3427, 2008.

[2] J. Bálbas and E. Tadmor. Non-oscillatory central schemes for one and two-dimensional magnetohydrodynamics II: High-order semi-discrete schemes. *SIAM. J. Sci. Comput.,* 28 (2), 533-560, 2006.

[3] J. Bálbas , E. Tadmor and C. C. Wu. Non-oscillatory central schemes for one and two-dimensional magnetohydrodynamics I. *J. Comp. Phys.,* 201 (1), 261-285, 2004.

[4] D. S. Balsara. Divergence free adaptive mesh refinement for magnetohydrodynamics. *J. Comp. Phys.*, 174:614-648, 2001.

[5] D. S. Balsara and D. Spicer. A staggered mesh algorithm using high order Godunov fluxes to ensure solenoidal magnetic fields in magnetohydrodynamic simulations. *J. Comp. Phys.*, 149(2):270-292, 1999.

[6] J. B. Bell, P. Colella and H. M. Glaz. A second-order projection method for the incompressible Navier-Stokes equations. *J. Comp. Phys.*, 85, 257-283, 1989.

[7] F. Bouchut, C. Klingenberg and K. Waagan. A multi-wave HLL approximate Riemann solver for ideal MHD based on relaxation I- theoretical framework. *Numer. Math.*, 108 (1), 7-42, 2007.

[8] J. U. Brackbill and D. C. Barnes. The effect of nonzero Div$B$ on the numerical solution of the magnetohydrodynamic equations. *J. Comp. Phys.*, 35:426-430, 1980.

[9] M. Brio and C. C. Wu. An upwind differencing scheme for the equations of ideal MHD. *J. Comp. Phys,* 75 (2), 1988, 400 - 422.

[10] A. J. Chorin. Numerical solutions of the Navier-Stokes equations. *Math. Comp.*, 22, 745-762, 1968.

[11] W. Dai and P. R. Woodward. A simple finite difference scheme for multi-dimensional magnetohydrodynamic equations. *J. Comp. Phys.*, 142(2):331-369, 1998.

[12] H. Deconnik, P. L. Roe and R. Struijs. A multi-dimensional generalization of Roe's flux difference splitter for Euler equations. *Comput. Fluids*, 22, 215, 1993.
[13] A. Dedner, F. Kemm, D. Kröner, C. D. Munz, T. Schnitzer and M. Wesenberg. Hyperbolic divergence cleaning for the MHD equations. *J. Comp. Phys.,* 175, 645-673, 2002.
[14] C. Evans and J. F. Hawley. Simulation of magnetohydrodynamic flow: a constrained transport method. *Astrophys. J.*, 332:659, 1998.
[15] M. Fey. Multi-dimensional upwingding.(I) The method of transport for solving the Euler equations. *J. Comp. Phys.,* 143(1): 159-180, 1998.
[16] M. Fey. Multi-dimensional upwingding.(II) Decomposition of Euler equations into advection equations. *J. Comp. Phys.,* 143(1): 181-199, 1998.
[17] F. Fuchs, S. Mishra and N.H. Risebro. Splitting based finite volume schemes for ideal MHD equations. *J. Comp. phys,*, 228 (3): 641-660, 2009.
[18] F. Fuchs, A. McMurry, S. Mishra, N. H. Risebro and K. Waagan. Finite volume methods for wave propagation in stratified magneto-atmospheres. *Comm. Comp. Phys.,* To appear.
[19] F. Fuchs, A. D. McMurry, S. Mishra, N. H. Risebro and K. Waagan. Approximate Riemann solver based high order finite volume schemes for the Godunov-Powell form of the ideal MHD equations in multi dimensions. *Preprint,* 2009.
[20] S. K. Godunov. The symmetric form of magnetohydrodynamics equation. *Num. Meth. Mech. Cont. Media*, 1:26-34, 1972.
[21] K. F. Gurski. An HLLC-type approximate Riemann solver for ideal Magneto-hydro dynamics. *SIAM. J. Sci. Comp.*, 25(6), 2004, 2165-2187.
[22] S. Gottlieb, C. W. Shu and E. Tadmor. High order time discretizations with strong stability property. *SIAM. Review,* 43, 2001, 89 - 112.
[23] A. Harten, B. Engquist, S. Osher and S. R. Chakravarty. Uniformly high order accurate essentially non-oscillatory schemes. *J. Comput. Phys.*, 1987, 231-303.
[24] A. Kurganov and E. Tadmor. New high resolution central schemes for non-linear conservation laws and convection-diffusion equations. *J. Comput. Phys*, 160(1), 241-282, 2000.
[25] B. van Leer Towards the Ultimate Conservative Difference Scheme, V. A Second Order Sequel to Godunov's Method. *J. Com. Phys.,* 32, 101136, 1979.
[26] R. J. LeVeque. Finite volume methods for hyperbolic problems. *Cambridge university press,* Cambridge, 2002.
[27] R. J. LeVeque. Wave propagation algorithms for multi-dimensional hyperbolic systems, *J. Comp. Phys.,* 131, 327-353, 1997.
[28] M. Lukacova-Medvidova, K. W. Morton and G. Warnecke. Evolution Galerkin methods for Hyperbolic systems in two space dimensions. *Math. Comp.,* 69 (232), 1355 - 1384, 2000.
[29] M. Lukacova-Medvidova, J. Saibertova and G. Warnecke. Finite volume evolution Galerkin methods for Non-linear hyperbolic systems. *J. Comp. Phys.,* 183, 533 - 562, 2003.
[30] T. J. Linde. *A three adaptive multi fluid MHD model for the heliosphere.* Ph.D thesis, University of Michigan, Ann-Arbor, 1998.
[31] S. Mishra and E. Tadmor, Constraint preserving schemes using potential-based fluxes. I. Multi-dimensional transport equations. *Preprint,* 2009.
[32] S. Mishra and E. Tadmor, Constraint preserving schemes using potential-based fluxes. II. Genuinely multi-dimensional central schemes for systems of conservation laws. *Preprint,* 2009.
[33] A. Mignone et. al. Pluto: A numerical code for computational astrophysics. *Astrophys. J. Suppl.*, 170, 2007, 228 - 242.
[34] T. Miyoshi and K. Kusano. A multi-state HLL approximate Riemann solver for ideal magneto hydro dynamics. *J. Comp. Phys.* 208 (1), 2005, 315 - 344.
[35] H. Nessyahu and E. Tadmor. Non-oscillatory central differencing for hyperbolic conservation laws. *J. Comp. Phys.,* 87 (2), 408 - 463, 1990.
[36] S. Noelle. The MOT-ICE: A new high-resolution wave propagation algorithm for multi-dimensional systems of conservation laws based on Fey's method of transport. *J. Comp. Phys.,* 164, 283 - 334, 2000.
[37] B. Perthame and C. W. Shu. On positivity preserving finite volume schemes for Euler equations. *Numer. Math.,* 73 (1), 119 - 130, 1996.
[38] K. G. Powell. An approximate Riemann solver for magneto-hydro dynamics (that works in more than one space dimension). Technical report, 94 -24, ICASE, Langley, VA, 1994.
[39] K. G. Powell, P. L. Roe. T. J. Linde, T . I. Gombosi and D . L. De zeeuw, A solution adaptive upwind scheme for ideal MHD. J. Comp. Phys, 154(2), 284 - 309, 1999
[40] P. L. Roe and D. S. Balsara. Notes on the eigensystem of magnetohydrodynamics. *SIAM. J. Appl. Math.*, 56 (1), 1996, 57 - 67.
[41] J. Rossmanith. A wave propagation method with constrained transport for shallow water and ideal magnetohydrodynamics. Ph.D thesis, University of Washington, Seattle, 2002.
[42] D. S. Ryu, F. Miniati, T. W. Jones and A. Frank. A divergence free upwind code for multidimensional magnetohydrodynamic flows. *Astrophys. J.*, 509(1):244-255, 1998.
[43] C. W. Shu and S. Osher. Efficient implementation of essentially non-oscillatory schemes - II, *J. Comput. Phys.*, 83, 1989, 32 - 78.

[44] E. Tadmor. Approximate solutions of nonlinear conservation laws. *Advanced Numerical approximations of Nonlinear Hyperbolic equations, A. Quarteroni ed.*, Lecture notes in Mathematics, Springer Verlag (1998), 1-149.
[45] M. Torrilhon and M. Fey. Constraint-preserving upwind methods for multidimensional advection equations. *SIAM. J. Num. Anal.*, 42(4):1694-1728, 2004.
[46] M. Torrilhon. Locally divergence preserving upwind finite volume schemes for magnetohyrodynamic equations. *SIAM. J. Sci. Comp.*, 26(4):1166-1191, 2005.
[47] G. Toth. The Div$B = 0$ constraint in shock capturing magnetohydrodynamics codes. *J. Comp. Phys.*,161:605-652, 2000.

(Siddhartha Mishra)
SAM, D-MATH, ETH Zürich,
HG G 57.2, Rämistrasse 101, Zürich-8092, Switzerland
E-mail address: siddharm@cma.uio.no

(Eitan Tadmor)
Department of Mathematics
Center of Scientific Computation and Mathematical Modeling (CSCAMM)
Institute for Physical sciences and Technology (IPST)
University of Maryland
MD 20741-4015, USA
E-mail address: tadmor@cscamm.umd.edu

Research Reports

No.	Authors/Title
09-33	*S. Mishra, E. Tadmor* Constraint preserving schemes using potential-based fluxes. III. Genuinely multi-dimensional central schemes for for MHD equations
09-32	*S. Mishra, E. Tadmor* Constraint preserving schemes using potential-based fluxes. II. Genuinely multi-dimensional central schemes for systems of conservation laws
09-31	*S. Mishra, E. Tadmor* Constraint preserving schemes using potential-based fluxes. I. Multidimensional transport equations
09-30	*D. Braess, S. Sauter, C. Schwab* On the justification of plate models
09-29	*D. Schötzau, C. Schwab, T. Wihler* *hp*-dGFEM for second-order elliptic problems in polyhedra. II: Exponential convergence
09-28	*D. Schötzau, C. Schwab, T. Wihler* *hp*-dGFEM for second-order elliptic problems in polyhedra. I: Stability and quasioptimality on geometric meshes
09-27	*A. Moiola, R. Hiptmair, I. Perugia* Approximation by plane waves
09-26	*M. Karow, E. Kokiopoulou, D. Kressner* On the computation of structured singular values and pseudospectra
09-25	*M. Durán, M. Guarini, C.F. Jerez-Hanckes* Hybrid FEM/BEM modeling of finite-sized photonic crystals for semiconductor laser beams
09-24	*A. Bespalov, N. Heuer, R. Hiptmair* Convergence of the natural *hp*-BEM for the electric field integral equation on polyhedral surfaces
09-23	*R. Hiptmair, J. Li, J. Zou* Real interpolation of spaces of differential forms
09-22	*R. Hiptmair, J. Li, J. Zou* Universal extension for Sobolev spaces of differential forms and applications
09-21	*T. Betcke, D. Kressner* Perturbation, computation and refinement of invariant pairs for matrix polynomials